Automatic Detection and Identification of Trichomonas Vaginalis from Fluorescence Microscopy Images

Yongjian Yu[1] and Jue Wang[2]

[1]*Axon Connected, LLC, Earlysville, VA 22936, U.S.A.*
[2]*Department of Mathematics, Union College, Schenectady, NY 12308, U.S.A.*

Keywords: Detection, Segmentation, Multiscale, Trichomoniasis, Trichomonas Vaginalis, Fluorescence Microscopy.

Abstract: Trichomonas vaginalis (TV) causes sexually transmitted infections that, if unresolved timely, can lead to adverse health conditions. We construct a software platform integrating a novel, robust multiscale image analysis pipeline for automatic detection and characterization of TV from dual-resolution, multi-band digital fluorescence microscopy scans. We develop two spectral indices to highlight the TV in the spectrally contaminated image. The system employs a search algorithm that incorporates the spectral indices to locate the microorganisms from the low-resolution scans across the sample slide, and then identifies the TV using a multiscale edge-sensitive automatic thresholding segmentation and index-driven ranking in the high-resolution view. Method capability is demonstrated through the discriminability in the feature classification and in the TV test pipeline, both showing a high sensitivity. This technique can be used to enable automatic, fast diagnosis of trichomoniasis at the point-of-care clinics.

1   INTRODUCTION

Trichomoniasis (or trich for short) is the most prevalent non-viral sexually transmitted infection (STI) in the world (Bahadory *et. al.* 2021; WHO 2021a). It is caused by infection with a protozoan parasite called Trichomonas vaginalis (T. vaginalis, or TV for short). In 2020, the World Health Organization (WHO) estimated 156 million new infections of trich (WHO 2021b). According to the latest WHO report, the estimates for trich were 6.3% (95% UI: 4.0–7.2) in women and 0.6% (95% UI: 0.4–0.9) in men (Rowley *et. al.* 2019). Because no recommendations are available for general screening for TV, the epidemiology of trich has largely come from population-based and clinic-based surveillance studies (CDC 2021).

TV infection can be overlooked by clinicians, as the process generally follows a benign course and is frequently asymptomatic. The majority of people who have trich (70–85%) either have minimal or no genital symptoms, and untreated infections might last from months to years (CDC 2021). Symptoms of TV may be non-specific, making it difficult to differentiate TV from other STIs clinically, which require different treatment approaches. TV infection in women is associated with vaginitis, urethritis, cervicitis, and pelvic inflammatory disease. TV infection can cause adverse pregnancy complica-

tions, such as tubal infertility, preterm delivery, low birth weight, and premature rupture of membranes (Webb *et. al.* 2021). TV transmission from mother to child has been associated with neonatal morbidities, including vaginitis, urinary tract infection, and respiratory disease. TV infection has also been linked to cervical human papillomavirus (HPV) infection and cervical cancer (Amorim *et. al.* 2017; Bahadory *et. al.* 2021). Among men, TV infection has been associated with benign prostatic hyperplasia and invasive prostate cancer (Bahadory *et. al.* 2021; Webb *et. al.* 2021). Moreover, TV infection is associated with an increased risk of human immunodeficiency virus (HIV) transmission and acquisition (Masha *et. al.* 2019). Up to 53% of women with HIV have TV infections (CDC 2021). Without inclusive testing protocols, TV infections largely go undiagnosed and untreated. Therefore, improving the detection of TV is of high significance and impact.

The standard test for trich at the near point-of-care (nPOC) clinics uses microscopic examinations of the fresh saline wet mount to identify moving organisms as TV. Wet mount microscopy is considered insensitive compared to the culture method (Nathan *et. al.* 2015). The sensitivity is reported to be 52% in a recent study of 136 participants (Hsieh *et. al.* 2020). Current screening for trich is performed using tests with limited

sensitivity, including wet mount microscopy (sensitivity 38–68%), culture of specimens (44–88%), nucleic acid hybridization (roughly 60%), rapid antigen detection (83–86%), and nucleic acid amplification tests (NAATs) (76–100%) (Andrea and Chapin 2011; CDC 2021; Gaydos *et. al.* 2017; Hsieh *et. al.* 2020; Hobbs and Seña 2013; Nathan *et. al.* 2015; Patil *et. al.* 2012). The culture method has a relatively longer turn-around time and is limited by non-viable organisms in the specimen. The FDA-cleared NAATs can improve the quality of trich diagnostics, but they use large robotic platforms and are time-consuming, thus not feasible for nPOC. Moreover, the result is typically yes or no, rather than being quantitative. The histochemical methods use non-specific stains, which require interpretations by the cytologists, pathologists, or other experts.

The emerging immunofluorescence (IF) assay that binds the trich specific molecules enables an easy interpretation and thus lowers the critical errors. The IF assay makes it possible to locate, highlight, and count all living, immobile, dead, and even partially destroyed TV. In addition, the IF assay is more sensitive than the wet mount brightfield microscopic examinations. An automatic IF assay equipped with motorized scanner and automatic data analyzer is highly desired. It is a challenging task to automatically detect the rare TV from the IF micrographs, especially in the early stage of infection. The TV is embedded among other microorganisms such as white blood cells, epithelial cells, yeast, hyphae, and swab debris, etc. The multiband image suffers from degradation due to channel crosstalk, local defocusing, biological sample variability, and preparation variability.

Example IF micrographs of clinical samples are shown in Figure 1 at a 4X objective and Figure 2 at a 40X objective, respectively. The color is assigned as follows: red for channel 3 (epithelial cells), green for channel 2 (yeast and hyphae of candida albicans), grayscale for channel 1 (nuclei of various microorganisms including the bacteria, epithelial cells, TV, white blood cells, and yeast), and blue for channel 4 (TV). The pseudo-color for display is different from the LED illumination or fluorophore emission waveband, which is further elaborated in section 2.1. The non-specific staining can be seen in the composite image. The TV is oval shaped and has a faint eccentric, elongated nucleus. The organism varies in size but is typically around 10 μm in length and 7 μm in width, slightly larger than the white blood cell (WBC). It can assume an amoeboid form when attached to the vaginal epithelial cells. Towards detection efficiency and robustness, the

algorithm needs to first find the TV candidates using a 4X objective, and then identify the TV within a 40X objective high-resolution view.

We propose two normalized TV spectral indices along with a pipeline of data processing algorithms for a rapid search and identification of TV from IF micrographs. We analyze the discriminability of the indices and demonstrate their potential after being integrated into an automated digital IF microscopic system for a computer-aided diagnosis of trich.
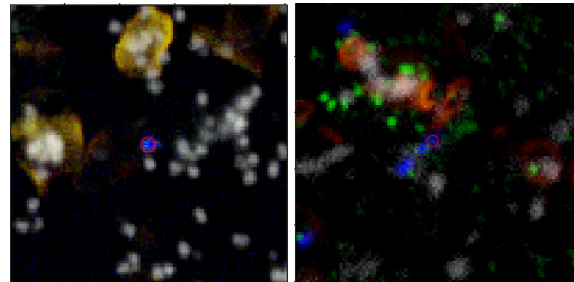

Figure 1: Composite images of pseudo-colored four-band IF micrographs at a 4X objective. The locations of possible TV (blue) are marked by the red circles.
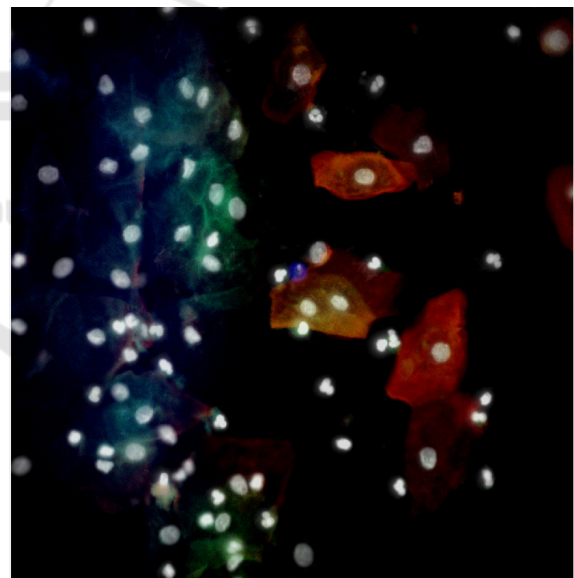

Figure 2: Composite image of pseudo-colored four-band IF micrograph at a 40X objective. The TV approximately centered in the image.

2 METHODS

2.1 Problem Statement

A research digital IF microscopic platform under development and optimization is utilized for this

study. The platform runs with dual resolutions, four spectral channels, and is configurable to scan and analyze vaginal microbiome swab samples for aiding diagnosis of bacterial vaginosis, candida albicans infection, and trichomoniasis (trich). The four-channel image can be expressed by

$$I = (I_1 \quad I_2 \quad I_3 \quad I_4). \qquad (1)$$

The I_1, I_2, I_3 and I_4 represent the fluorescence images in the four emission spectral channels (lime, green, blue, and far red). The LED illumination spectrum for each channel image is at a shorter wavelength than the respective stain emission wavelength. These images contain numerous different microorganisms, in the form of isolated cells or colony of cells, such as the epithelium, fungus, DNA materials/bacteria, and TV. For the diagnosis of trich, a TV-specific antibody staining enables TV expression mostly in I_4. Likewise, I_3, I_2, and I_1 express selectively the stained epithelium, fungus, and DNA materials/bacteria, respectively. Because of the channel crosstalk problem, these images are not mutually independent in terms of the contents. In the TV expression channel I_4, there exist distractive interfering images of irrelevant objects. Likewise, the other channels have their own latent objects of interest, but also contain the ghost images of the other unwanted objects. The presence of channel crosstalk reduces the sensitivity and accuracy of finding, segmenting, and identifying TV. Detection of TV with a high sensitivity becomes a challenging task in the case of only a single TV presence. The difficulty is further compounded by the background fluorescence and debris that increase the false detection rate.

2.2 Segmentation and Identification

The dual-resolution system uses a 4X and a 40X objective to find and identify the TV, respectively.

2.2.1 TV Search

A 4X scan of the sample slide yields 25 sub-images, each with 2K-by-2K pixels. The pixel pitch of the image is approximately 1.6 μm. The 4X TV search algorithm consists of finding the boundary of the organism and its nucleus, blob quantification, and support vector machine (SVM) classification of the blobs into two classes: TV alike and non-TV.

The external boundary segmentation of TV is performed via adaptive thresholding of the TV-sensitive channel 4X I_4. Considering the tiny size of the trich nucleus (1 to 3 pixels), we apply the top-hat
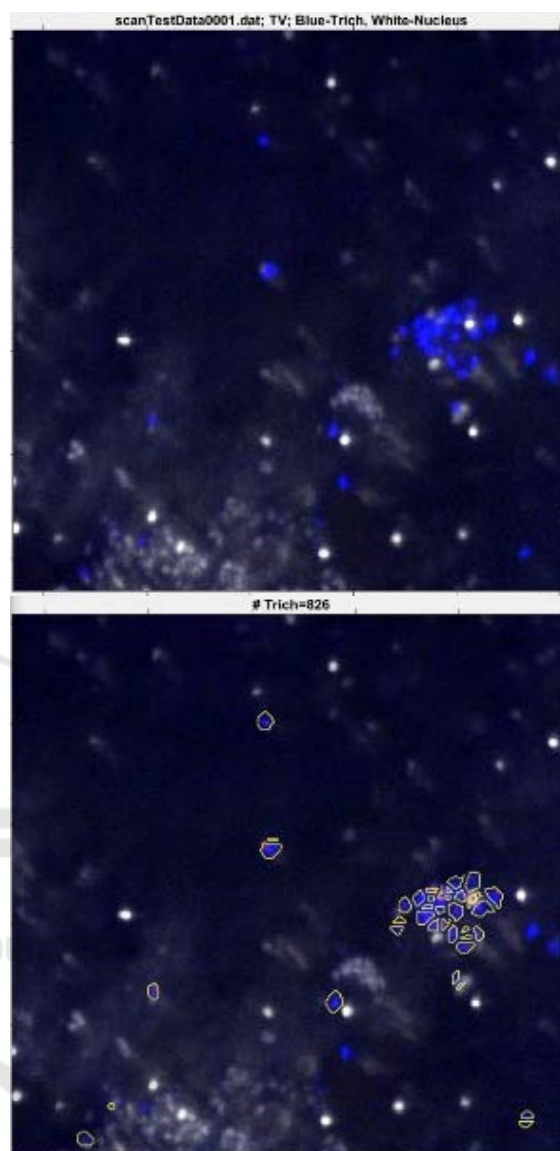

Figure 3: 4X TV search and segmentation. The contour delineates the TV external boundary.

filtering of DNA-sensitive channel 4X I_1 for bright objects to extract the trich nuclei. Top-hat filtering computes the morphological opening of the image and then subtracts the result from the original image. The TV candidates are masked as nucleated blobs in the 4X I_4 segmentation map. Any clump of nuclei is identified by a size thresholding and then split into individual TV nucleus using a marker-controlled watershed method. The nuclear markers are located as the local extended maxima. Similarly, a touching cluster of TV is identified by the number of nuclei in the cluster and spilt via the watershed controlled by the individually segmented nucleus. Finally, the

strong cytokeratin and yeast areas are masked out using a set union:

$$H(I_3 - I_1 + \varepsilon) \cup H(I_2 - I_1 + \varepsilon), \qquad (2)$$

where $H(\cdot)$ is the Heaviside function acting as a thresholding operator; the $\cup$ denotes the union of sets; ε is a smaller number in the range of 0-10. An example of the 4X TV segmentation is shown in Figure 3.

The initial TV candidates are numerically labelled. Each blob will be further quantified by the features outlined in the later sections and classified into TV alike or non-TV. Each 4X TV candidate is then imaged with a 40X objective and examined to identify if it is a true TV.

2.2.2 TV Segmentation with Multiscale Edge-sensitive Automatic Thresholding

In order to accommodate for the shadow depth of focus with the 40X objective imaging, which may cause the local out-of-focus issue, we develop a multiscale edge-sensitive automatic thresholding technique for 40X TV segmentation. The edge information facilitates locating the objects in dim regions where they are likely to be missed by grayscale thresholding, and the automatic thresholding recovers the cells with undefined edges due to local defocusing. The method optimizes an objective functional, i.e., maximizing the Dice shape similarity between the multiscale edge synthesized segmentation and automatic thresholding segmentation of an input image I, expressed as follows,

$$T^* = \max_T \frac{|H(\tilde{I} - T) \cap F(C)|}{|H(\tilde{I} - T)| + |F(C)|}, \qquad (3)$$

where $\tilde{I}$ is an L-level linear quantized image of I (40X I_4 or I_1); the quantization compresses the range of the threshold value T to an integer set $\{1, 2, \ldots, L\}$. $H(\cdot)$ is the Heaviside function acting as a thresholding operator. C denotes the edge synthesized contours by morphological linking of the multiscale edges E of the input image I, $C = (E \oplus S_\parallel) \oplus S_\perp$, where $\oplus$ stands for the dilation operator; $S_\parallel$ and $S_\perp$ are the horizontal and vertical line structure elements of length 3, respectively; $F(\cdot)$ is the filling operator on C. The final 40X TV segmentation is given by the fusion $H(\tilde{I} - T^*) \cup F(C)$.

The morphological linking synthesized edge C may contain false contours resulted from the clustered edges of noise. Moreover, the algorithm

itself is unable to determine if the segmentation is good or bad without the ground truth. To overcome these issues, we build and incorporate some ground truth data into the proposed segmentation paradigm.

In recognition of the approximate circular shape prior of the objects of interest, we perform a circular Hough transform to I to find all circles with radii in the radius range of TV (or TV nuclei if segmenting the TV nuclei). This results a network of circles C_0. Since C_0 is much resilient to image noise and fuzzy edges, $F(C_0)$ is well deserved to be an approximate ground truth semantic segmentation. We regularize $F(C)$ using $F(C_0)$ by maintaining only the segmentations in $F(C)$ that are also in $F(C_0)$. When the foreground is well segmented, the shapes of $F(C)$ and $F(C_0)$ are close to each other, leading to a high shape similarity. When C deviates from C_0 significantly, C becomes unreliable. We set the Dice metric threshold of 0.5 for an acceptable goodness measure of C with reference to C_0. If the Dice metric is below 0.5, we use C_0 rather than C as the final object segmentation.

The edge-sensitive automatic thresholding segmentation with shape regularization and approximate ground truth support solves the problem (to a certain extent) of conventional segmentation algorithms (Ray and Saha 2007), where the algorithms are unable to tell if the results are satisfactory or not unless a human user inspects the results.

2.3 Normalized Tv Spectral Indices

Denote J_k the latent fluorescence signal in the raw image I_k (k =1 to 4). The raw signal in the kth channel can be modelled as a linear combination of the latent data across four channels,

$$I_k = \sum_{l=1}^{4} \alpha_{kl} J_l + n_k, \qquad (4)$$

where α_{kl} is a 4 by 4 real-coefficient matrix, with unity diagonal elements, i.e., $\alpha_{kk} = 1$; n_k is the background and noise. The off-diagonal non-zero coefficients reflect the residual of channel crosstalk, non-specific staining, and sample variability.

The research microscope system in use does not provide channel crosstalk correction, and thus the latent image is inaccessible. To solve the channel crosstalk problem with the raw data, we proposed two spectral indices for a robust search of TV alike with a low-resolution view, followed by quality verification with a high-resolution view. A pre-processing is first performed to convert the raw image into an image appropriate for human

visualization of the targets of interest, including noise reduction, contrast enhancement, and background subtraction. The TV spectral indices are defined as

$$\mathrm{TVSI}_1 = (\hat{I}_4 - \hat{I}_1)/(\hat{I}_4 + \hat{I}_1), \qquad (5)$$

$$\mathrm{TVSI}_2 = (\hat{I}_4 - \hat{I}_2)/(\hat{I}_4 + \hat{I}_2), \qquad (6)$$

where $\hat{I}_k = p(I_k)$, $k = 1$ to 4; $p(I)$ denotes a series of operations on I, including the median filtering, histogram stretching, and background subtraction. The denominators in (5) and (6) normalize the spectral indices to highlight the dim TV by suppressing the distractive interference of ghost images of unwanted objects. Both indices are less than 1, but they can assume small negative values because the illumination in each channel is unbalanced. In section 3 results, we will mainly demonstrate the discriminability of these two indices, coupled with other features, for TV search and identification.

2.4 TV Ranking for Identification

The TV is of similar size with many district clutter organisms, such as the (candida albicans) yeast cells, monocytes, and some debris co-existing in the trich test sample. These clutter organisms express fluorescence in the same waveband as the TV does. Consequently, accurate TV enumeration is hindered by the false positive rate resulted from misidentifying those yeast cells, monocytes and debris as TV. To increase the accuracy of trich diagnosis, we develop a TV ranking model to differentiate quantitatively the detected TV from yeast or debris. This model incorporates the spectral indices, sizes of TV and its nucleus, and a condition that the TV must have a nucleus.

The DNA marker channel I_1 is first enhanced around the 4X candidate region using a multiscale blobness filter bank, followed by a binarization of the blobness image using the clustering method (Otsu 1979), biovolume elasticity method (Luo *et. al.* 2018), or locally adaptive thresholding method (Singh *et. al.* 2011). The binarized map contains the TV nucleus, as well as other DNA materials (e.g., nuclei of WBC), which may cluster with the TV nucleus under examination. The nuclear clumps are split using the watershed transform. Denote B_t and B_n the segmentation masks of TV and its nucleus, respectively. B_t is further split until each area has one nucleus in it. The true TV nucleus is determined via a merit scoring and selection process. The ranking model is defined by

$$R = S\left(\frac{\langle \mathrm{TVSI}_1 \rangle - \mu_1}{\sigma_1}\right) S\left(\frac{\langle \mathrm{TVSI}_2 \rangle - \mu_2}{\sigma_2}\right)$$
$$f(B_t, B_n) g(A_t, A_n; M_t, M_n, D_t, D_n), \qquad (7)$$

where $S(\cdot)$ is the Sigmoid function parametrized by the offset μ and spread σ; $\langle \cdot \rangle$ denotes the averaging of cell segmentation; $f(B_t, B_n) = |B_t \cap B_n|/|B_n|$; the $\cap$ and $|\cdot|$ denote set intersection and cardinality, respectively; $g(A_t, A_n; M_t, M_n, D_t, D_n)$ is the size driven probability given by

$$g(A_t, A_n; M_t, M_n, D_t, D_n) =$$
$$\exp\left(-\frac{(A_t - M_t)^2}{2D_t{}^2}\right) \exp\left(-\frac{(A_n - M_n)^2}{2D_n{}^2}\right), \qquad (8)$$

where A_t and A_n are the trich area and nucleus area, respectively; M_t, M_n, D_t, D_n are the means and standard deviations of the sizes of TV and nucleus, respectively.

3 RESULTS

We demonstrate the capability and power of the proposed platform for TV testing. Firstly, the spectral indices are employed as the discriminative features in the classification framework for TV and non-TV organisms. Secondly, the spectral indices, segmentation and ranking algorithms are integrated into a complete system for TV quantification.

In order to study how the normalized TV spectral indices perform as features for TV classification at a low resolution (4X objective), we construct four discriminative feature sets as follows:

$S_1 = \{\langle \mathrm{TVSI}_1 \rangle, \langle \mathrm{TVSI}_2 \rangle, \langle \hat{I}_4 \rangle\}$,

$S_2 = \{\langle \mathrm{TVSI}_1 \rangle, \langle \mathrm{TVSI}_2 \rangle, \langle \hat{I}_4 \rangle, \langle \hat{I}_1 \rangle\}$,

$S_3 = \{\langle \mathrm{TVSI}_1 \rangle, \langle \mathrm{TVSI}_2 \rangle, \langle \hat{I}_4 \rangle, \langle \hat{I}_1 \rangle, A_t, A_n\}$,

S_4 = Union of S_3 and {nucleus eccentricity, cell-minor-to-major-axis-length ratio}.

The nucleus eccentricity measures the distance between the centroid of the cell and nucleus. We apply the t-Distributed Stochastic Neighbor Embedding (t-SNE) to visualize the clusters of feature points in a two-dimensional plane based on the feature relative similarities in a high-dimensional feature space that corresponds to the user labels. The optimal feature set S_3 is identified with t-SNE; the result is shown in Figure 4. Using S_3, we train a linear and a nonlinear SVM classifier over 64 4X cell images that contain 31 TV positive and 33 TV negative. The samples are split randomly to 85% (54) training and 15% (10) testing. An accuracy of 90% is achieved for the linear SVM and the

accuracy increases to 100% with the nonlinear SVM using a radial basis function (RBF) kernel.

The TV detection and segmentation result at a high resolution is shown in Figure 5 (b), with a probability of 0.89 according to the ranking model. The normalized spectral index maps are illustrated in Figure 5 (c) and (d) that highlight the TV. A region of interest (ROI) is selected for processing. The procedure of nucleus detection and segmentation is illustrated in Figure 6.

To quantify the performance of the integrated IF system, 33 clinical TV samples are scanned and analyzed. Slide preparation takes places in the slide well. The sample is fixed with methanol for 5 minutes. A dilated solution of α-T. vaginalis, p65 adhesive antigen antibody is applied. The sample is incubated for 15 minutes at room temperature. Then DAPImount is applied and covered with a coverslip. The overall time for slide preparation is less than 30 minutes including wash and dry time. The sample slide is automatically scanned and trichomonads are enumerated and reported in about 15 minutes.

The test results are compared to the experts' data reading. The sensitivity of the IF TV test is 100%, specificity is 94%, and accuracy is 97%. We point out that the relative lower classification accuracy in the 4X classification is compensated by the 40X ranking mechanism thus a high overall system level performance is expected. The method comparison is summarized in Table 1. Compared to the standard wet mount microscopy and other methods used for trich diagnosis, the IF test achieves a superior performance. Coupling the 4X and 40X algorithms in the sample evaluation, the developed technique is able to deliver a test with a high sensitivity and accuracy for quick TV detection and identification.

Table 1: Comparison of sensitivity.

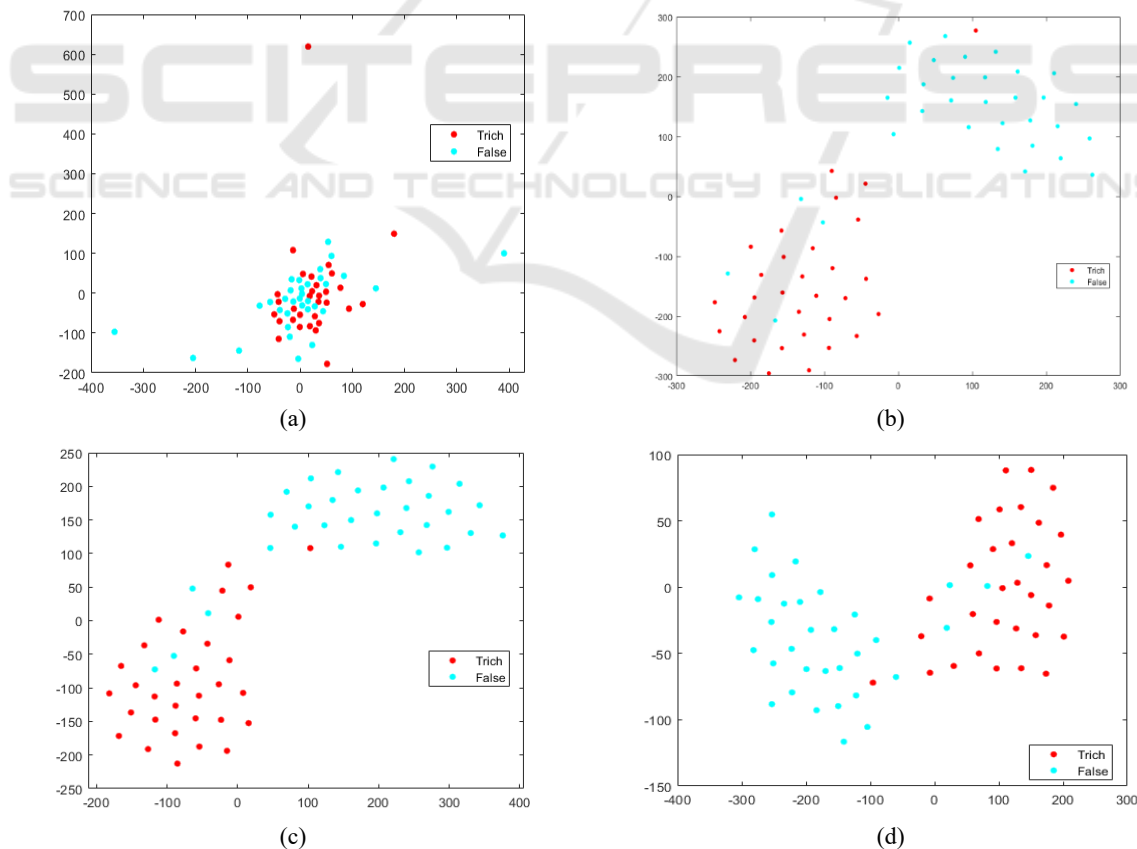| Wet mount microscopy	38–68%
Culture	44–88%
Nucleic acid hybridization	roughly 60%
Rapid antigen detection	83–86%
Nucleic acid amplification tests	76–100%
Proposed integrated IF	100%

Figure 4: Classification of TV and other cells using the discriminative features. (a) Three-feature set S_1. (b) Four-feature set S_2. (c) The optimal six-feature set S_3. (d) All eight features S_4.
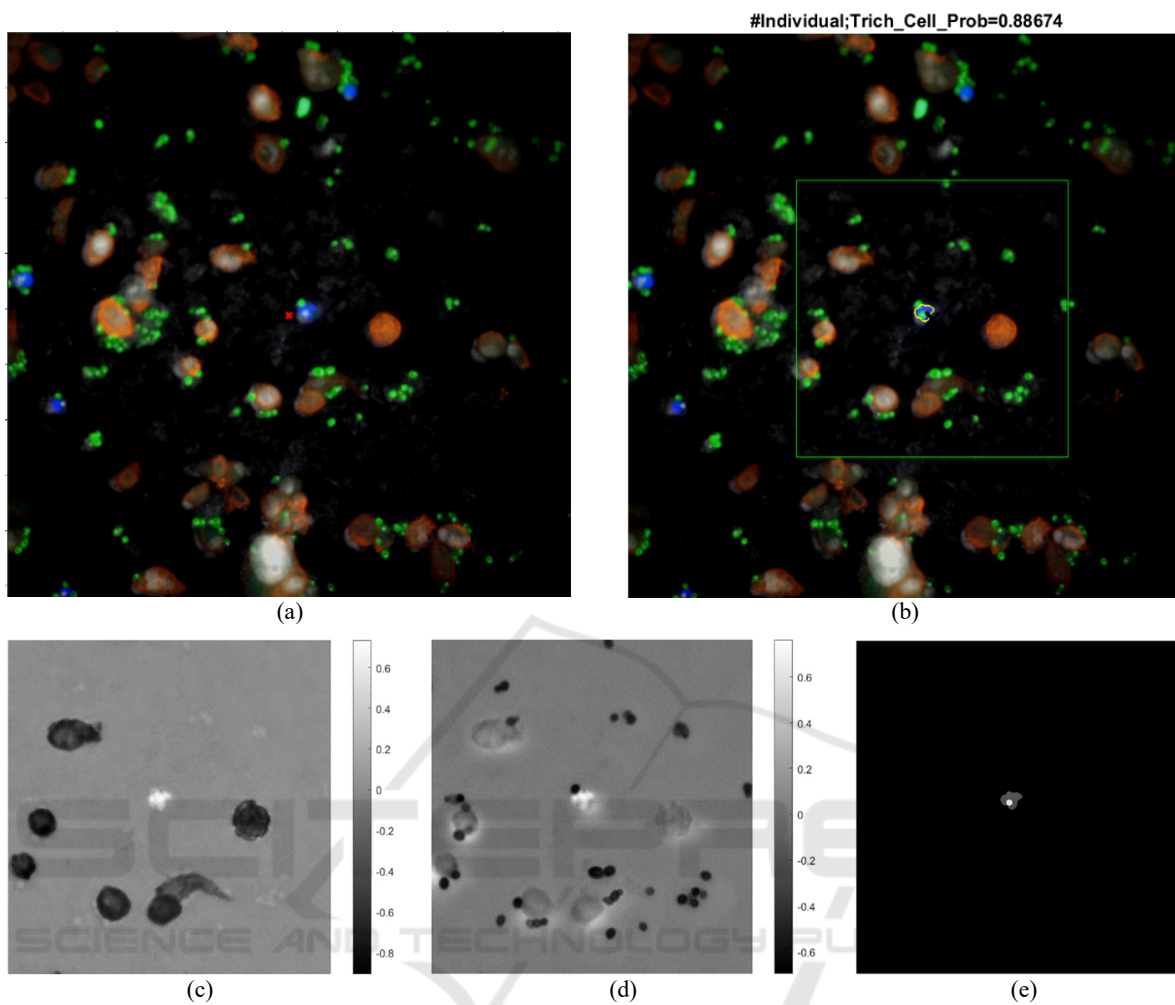
Figure 5. (a) Composite image of the pseudo-colored four-band IF micrograph at a 40X objective. (b) Segmentation contours of the TV and its nucleus, with the ROI box overlaid on the composite image. (c) Spectral index $TVSI_1$ map. (d) Spectral index $TVSI_2$ map. (e) Segmentation masks of the TV (gray) and its nucleus (white).
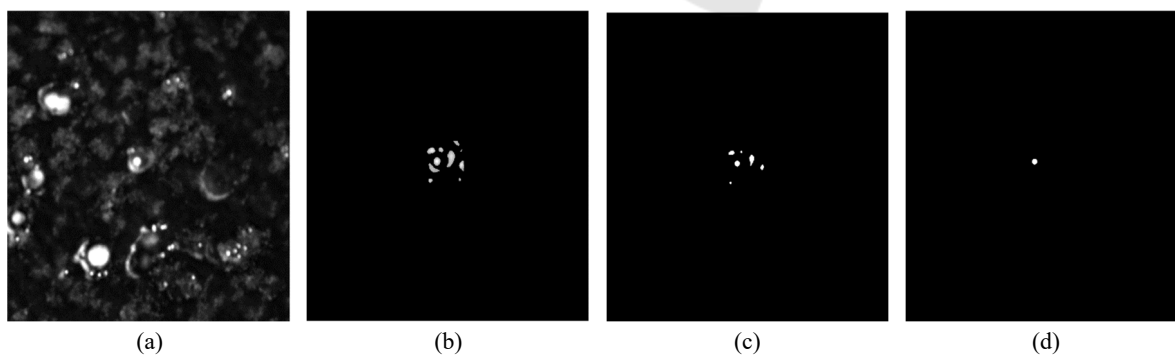

Figure 6: (a) Preprocessed nucleus channel. (b) ROI blobness enhancement. (c) Blobness map. (d) TV nucleus.

4 CONCLUSIONS

We have developed a set of novel spectral indices along with cell segmentation and ranking algorithms for a quick, robust search and quantitative identification of TV from fluorescence micrographs of specimen samples for assisting trich diagnosis in a point-of-care setting. We demonstrate that the proposed spectral indices are strong discriminative TV features against artifacts. A low-resolution search algorithm and a high-resolution identification algorithm are integrated into the testing framework and data processing pipeline. We devise an edge-sensitive automatic thresholding method that incorporates a cost minimization with an implicit shape regularization and self-validation. It is capable of extracting the TV with a wide range of signal levels and edge strengths. Moreover, this method is generic for cell detection. Our technique has shown promising results and achieved a high sensitivity and accuracy. We implement a software system that eliminates user variability in slide reading and offers the ability to archive images. The system enables a real-time, more accurate assessment of trich infections.

REFERENCES

A. T. Amorim, L. M. Marques, G. B. Campos, et al., "Co-infection of sexually transmitted pathogens and Human Papillomavirus in cervical samples of women of Brazil", *BMC Infect. Dis.*, 17(1):769, 2017.

S. B. Andrea and K. C. Chapin, "Comparison of Aptima Trichomonas vaginalis transcription-mediated amplification assay and BD Affirm VPIII for detection of T. vaginalis in symptomatic women: performance parameters and epidemiological implications", *J. Clin. Microbiol.*, 49(3):866-869, 2011.

S. Bahadory, S. Aminizadeh, A. Taghipour, F. Bokharaei-Salim, K. Khanaliha, M. H. Razizadeh, A. Soleimani, L. beikzadeh and A. Khatami, "A systematic review and meta-analysis on the global status of Trichomonas vaginalis virus in Trichomonas vaginalis", *Microbial Pathogenesis*, Vol. 158, 105058, 2021.

Centers for Disease Control and Prevention (CDC), Trichomoniasis, Sexually Transmitted Infections Treatment Guidelines, 2021.

C. A. Gaydos, J. D. Klausner, N. P. Pai, H. Kelly, C. Coltart and R. W. Peeling, "Rapid and point-of-care tests for the diagnosis of Trichomonas vaginalis in women and men", *Sex Transm. Infect.*, 93(S4):S31-S35, 2017.

M. M. Hobbs and A. C. Seña, "Modern diagnosis of Trichomonas vaginalis infection", *Sex Transm. Infect.*, 89(6):434-438, 2013.

Y. H. Hsieh, M. K. Lewis, V. G. Viertel, D. Myer, R. E. Rothman and C. A. Gaydos, "Performance evaluation and acceptability of point-of-care Trichomonas vaginalis testing in adult female emergency department patients", *Int. J. STD AIDS*, 31(14):1364-1372, 2020.

T. L. Luo, M. C. Eisenberg, M. A. L. Hayashi, C. Gonzales-Cabezas, B. Foxman, C. F. Marrs and A. H. Rickard, "A sensitive thresholding method for confocal laser scanning microscope image stacks of microbial biofilms", *Sci. Rep.*, Vol. 8, 13013, 2018.

S. C. Masha, P. Cools, E. J. Sanders, M. Vaneechoutte and T. Crucitti, "Trichomonas vaginalis and HIV infection acquisition: a systematic review and meta-analysis", *Sexually Transmitted Infections*, 95(1):36-42, 2019.

B. Nathan B, J. Appiah J, P. Saunders, D. Heron, T. Nichols, R. Brum, S. Alexander, P. Baraitser and C. Ison, "Microscopy outperformed in a comparison of five methods for detecting Trichomonas vaginalis in symptomatic women", *Int. J. STD AIDS*, 26(4):251-256, 2015.

N. Otsu, "A Threshold Selection Method from Gray-Level Histograms", *IEEE Trans. Syst. Man Cybern. Syst.*, Vol. 9, No. 1, 62-66, 1979.

M. J. Patil, J. M. Nagamoti and S. C. Metgud, "Diagnosis of trichomonas vaginalis from vaginal specimens by wet mount microscopy, in pouch tv culture system, and PCR", *J. Glob. Infect. Dis.*, 4(1):22-5, 2012.

N. Ray and B. Saha, "Edge sensitive variational image thresholding", *IEEE ICIP*, 16-19, 2007.

J. Rowley, S. Vander Hoorn, E. Korenromp, N. Low, M. Unemo, L. J. Abu-Raddad, R. M. Chico, A. Smolak, L. Newman, S. Gottlieb, S. S. Thwin, N. Broutet and M. M. Taylor, "Chlamydia, gonorrhoea, trichomoniasis and syphilis: global prevalence and incidence estimates, 2016", *Bulletin of the World Health Organization*, 97(8), 548-562P, 2019.

T. R. Singh, S. Roy, O. I. Siggh, T. Sinam and K. M. Singh, "A new local apative thresholding technique in binarization", *IJCSI International Journal of Computer Science Issues*, Vol. 8, Issue 6, No. 2, 271-277, 2011.

B. Webb, A. Crampton, M. J. Francis, J. Hamblin, T. M. Korman and M. Graham, "Increased diagnostic yield of routine multiplex PCR compared to clinician requested testing for detection of Trichomonas vaginalis", *Pathology*, Vol. 53, Issue 2, 257-263, 2021.

World Health Organization (WHO), "Global progress report on HIV, viral hepatitis and sexually transmitted infections", July 2021.

World Health Organization (WHO), "Sexually transmitted infections (STIs)", Nov. 2021.